Chapter 3

Coherence Cloning using SCL-OPLLs

3.1 Introduction

Narrow linewidth fiber lasers and solid state lasers have important applications in the area of fiber-optic sensing, interferometric sensing, LIDAR etc. SCLs are smaller, less expensive and inherently more efficient compared to fiber lasers, dye lasers and solid state lasers. However, they are much noisier due to their small volumes and the low reflectivity of the waveguide facet. The coherence of a high quality master laser, such as a narrow-linewidth fiber laser, can be cloned on to a number of noisy SCLs using OPLLs [81] as shown in figure 3.1. The cloning of the coherence of a single master laser to a number of slave SCLs has important consequences for sensor networks which require a large number of spectrally stabilized laser sources. To appreciate the benefits of this approach, we note that a commercial high-quality fiber laser has a cost of $10,000–$25,000, while an SCL typically costs a few hundred dollars, and the OPLL is constructed using inexpensive electronic components. The SCL typically also has a greater output power.

In this chapter, we describe the theoretical and experimental study of coherence cloning of a spectrally stabilized fiber laser to a high power commercial semiconductor DFB laser using an OPLL. We will further analyze the impact of coherence cloning on the observed spectrum in a self heterodyne Mach Zehnder interferometer (MZI).

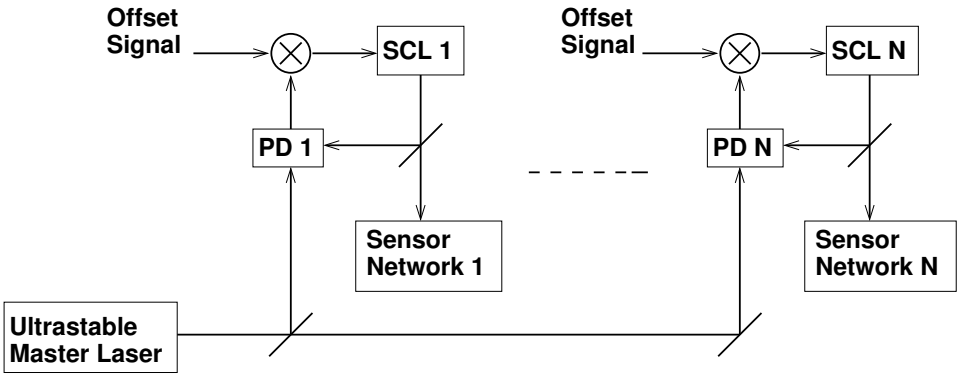

Figure 3.1. Individual SCLs all lock to a common narrow-linewidth master laser, thus forming a coherent array. An offset RF signal is used in each loop for additional control of the optical phase. PD: Photodetector.

Such an experiment is very common and is used for laser lineshape characterization, as well as applications such as interferometric sensing and FMCW LIDAR. We will show that the coherence-cloned slave SCL can act as a substitute for the master laser in the experiment.

3.2 Notation

For any wide sense stationary random process $x(t)$,

- The autocorrelation function is denoted by $R_x(\tau) = \langle x(t)\, x(t-\tau) \rangle$, where $\langle . \rangle$ denotes averaging over the time variable t. It is assumed that time and ensemble averages can be used interchangeably for the random processes considered in this chapter.

- The power spectral density is denoted by $S_x(f)$. From the Wiener-Khintchine theorem, $R_x(\tau)$ and $S_x(f)$ form a Fourier transform pair. In this chapter, we will work with two-sided power spectral densities.

- The variance of $x(t)$ is denoted by σ_x^2. If x is a function of another variable $x(t, \tau)$, we denote its variance by $\sigma_x^2(\tau)$.

3.3 Coherence Cloning in the Frequency Domain

From the small-signal model of the OPLL in figure 2.2(b) and equation (2.12), and ignoring the phase noise of the offset signal, we derive the following expression for the spectral density of the phase of the phase-locked slave SCL:

$$S_\nu^s(f) = S_\nu^m(f)\left|\frac{G_{op}(f)\cos\phi_{e0}}{1+G_{op}(f)\cos\phi_{e0}}\right|^2 + S_\nu^{s,fr}(f)\left|\frac{1}{1+G_{op}(f)\cos\phi_{e0}}\right|^2 + f^2\frac{S_{RIN}^m(f)}{4}\left|\frac{G_{op}(f)\sin\phi_{e0}}{1+G_{op}(f)\cos\phi_{e0}}\right|^2, \quad (3.1)$$

where $S_\nu^m(f)$, $S_\nu^{s,fr}(f)$ and $S_{RIN}^m(f)$ are the spectral densities of the frequency noise the master laser, the frequency noise of the free-running slave laser, and the RIN of the master laser respectively. From equation (3.1), we find that for frequencies smaller than the loop bandwidth, where $|G_{op}(f)| \gg 1$, the phase noise of the SCL tracks the phase noise of the master laser. For frequencies greater than the loop bandwidth, $|G_{op}(f)| < 1$, and the SCL phase noise reverts to the free-running level. This phenomenon is referred to as coherence cloning.

3.3.1 Experiment

A commercial DFB laser (JDS-Uniphase) is phase-locked to a narrow-linewidth fiber laser (NP Photonics) at an offset of 1.5 GHz using a heterodyne OPLL, as described in chapter 2, and the standard deviation of the residual phase noise is measured to be about 0.32 rad. The phase noise of the master fiber laser and the free-running and phase-locked DFB slave laser are characterized using two measurements. The lineshapes of the lasers are measured using a delayed self heterodyne interferometer with interferometer delay time much larger than the laser coherence time [83]. The frequency noise spectra of the lasers are also directly measured using a fiber MZI as a frequency discriminator [80].

The measured lineshapes of the fiber laser, and the free-running and locked DFB slave laser are plotted on a 50 MHz span in and a 500 kHz span in figure 3.2. The linewidth of the locked DFB laser is the same as that of the fiber laser for frequencies

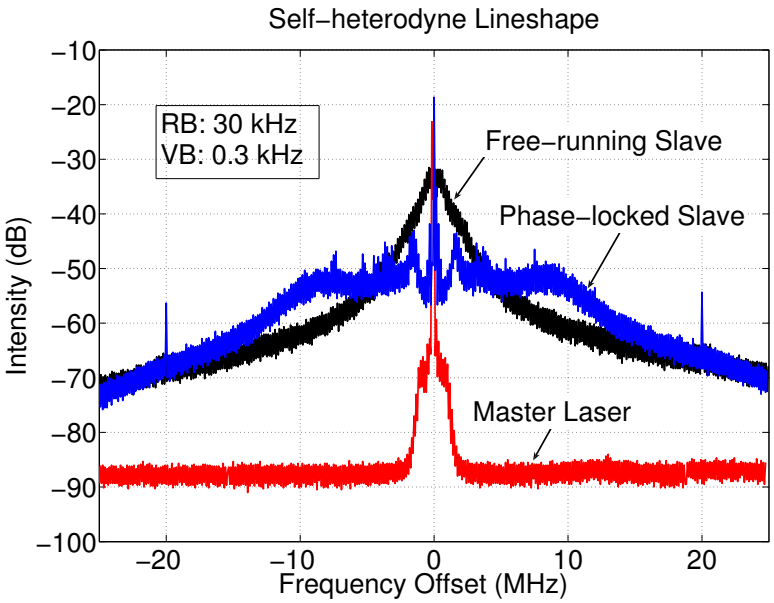

(a)

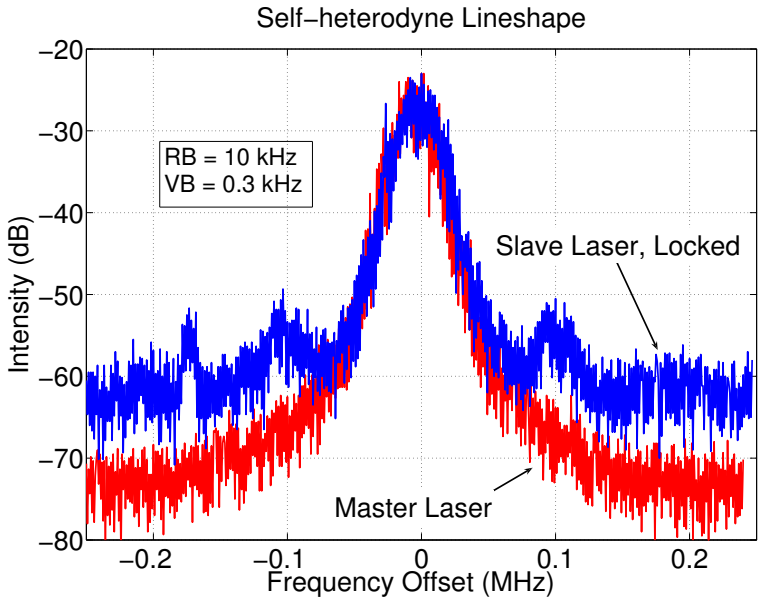

(b)

Figure 3.2. Measured linewidths of the master fiber laser, and the free-running and phase-locked slave SCL.

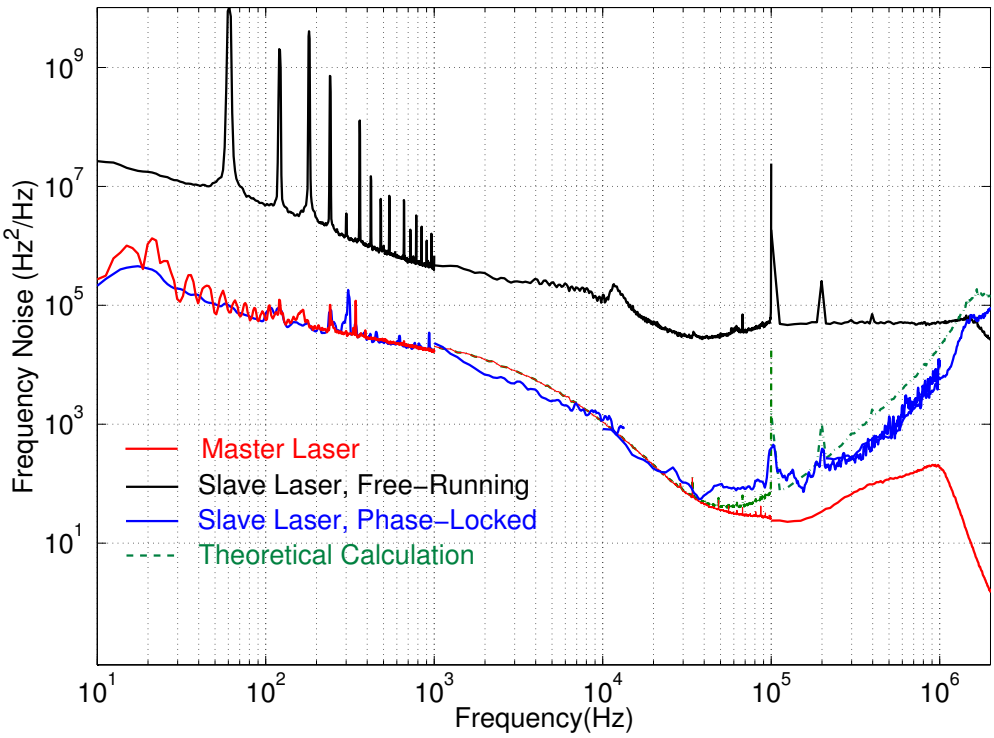

Figure 3.3. Measured frequency noise spectra of the master fiber laser, and the free-running and phase-locked slave DFB semiconductor laser. The green curve is the theoretical calculation of the frequency noise spectrum of the phase-locked slave laser using equation (3.1) and the measured loop parameters.

less than 50 kHz. Above 50 kHz, the linewidth of the locked DFB laser does not completely track the fiber laser due to the limited bandwidth of the OPLL. The 20 dB linewidth of the DFB laser is reduced from 4.5 MHz to 30 kHz.

The measured frequency noise spectra of the master fiber laser and the free-running and locked slave DFB SCL are shown in figure 3.3. The measured frequency noise (blue curve) of the locked DFB laser agrees well with the theoretical calculation (green curve) using equation (3.1). The frequency noise of the locked DFB laser is identical to that of the fiber laser for Fourier frequencies less than 50 kHz, which is consistent with the observation of the lineshapes in figure 3.2(b).

We see, therefore, that the DFB laser inherits the linewidth and frequency noise of the master laser when phase-locked using a heterodyne OPLL. However the coherence cloning is limited to frequencies within the bandwidth of the OPLL.

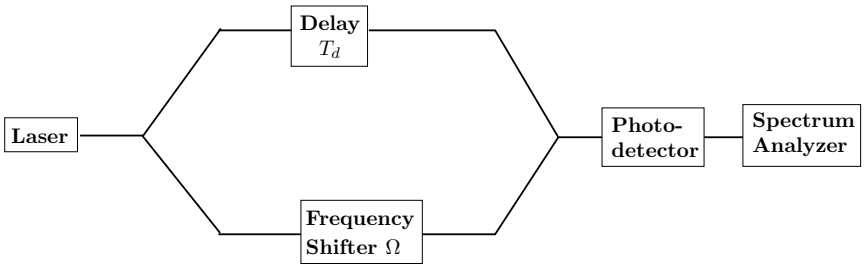

Figure 3.4. Delayed self-heterodyne interferometer experiment

3.3.2 Coherence Cloning and Interferometer Noise

We will now consider the effect of a limited-bandwidth coherence cloning experiment on interferometer noise. In particular, we will consider the Mach Zehnder interferometer (MZI) shown in figure 3.4. The laser output is split into two arms of MZI with a differential delay T_d. One of the arms also has a frequency shifter, such as an electro-optic or acousto-optic modulator that shifts the frequency of the optical field by Ω. This delayed self-heterodyne configuration is very common in a number of applications such as laser lineshape characterization, interferometric sensing and FMCW LIDAR. The laser field is given by $e(t) = a(t)\, e^{j\omega_0 t + \phi(t)}$, where $a(t)$ is the amplitude of the electric field, ω_0 the frequency of the laser, and $\phi(t)$ the laser phase noise. The output of the photodetector in figure 3.4 is given by

$$i(t) = \rho \left| e(t) e^{j\Omega t} + e(t - T_d) \right|^2 . \tag{3.2}$$

The intensity noise of the laser is typically much smaller than the detected phase noise and is neglected in this analysis. Further, without loss of generality, we let $\rho = 1$ and $|a(t)| = 1$ so that the photodetector current (around Ω) is given by

$$\begin{aligned} i(t) &= \Re\left(e^{j[(\omega_0+\Omega)t + \phi(t)]}\, e^{-j[\omega_0 (t-T_d) + \phi(t-T_d)]} \right) \\ &= \Re\left(e^{j\omega_0 T_d}\, e^{j\Omega t}\, e^{j\Delta\phi(t,T_d)} \right), \end{aligned} \tag{3.3}$$

where $\Delta\phi(t, T_d) \doteq \phi(t) - \phi(t - T_d)$ is the accumulated phase in the time interval $(t - T_d, t)$. We wish to investigate the effect of coherence cloning on the spectrum of

the electric field $e(t)$ and the photocurrent $i(t)$.

3.3.2.1 Coherence Cloning Model

Spontaneous emission in the lasing medium represents the dominant contribution to the phase noise $\phi(t)$ in a free-running semiconductor laser [88]. This gives rise to a frequency noise $\nu(t) = d/dt\,(\phi/2\pi)$ that has a power spectral density

$$S_\nu(f) = \frac{\Delta\nu}{2\pi}, \tag{3.4}$$

which in turn leads to a Lorenzian spectrum for the laser electric field, with full width at half maximum (FWHM) $\Delta\nu$. In practice, there are also other noise sources that give rise to a $1/f$ frequency noise at lower frequencies, as can be seen from figure 3.3. It has been shown [89] that the optical field spectrum of a laser with $1/f$ frequency noise has a Gaussian lineshape as opposed to a Lorenzian lineshape. For simplicity of analysis, we will assume in this chapter that the master and the free-running slave laser have flat frequency noise spectra corresponding to Lorenzian lineshapes with FWHMs $\Delta\nu_m$ and $\Delta\nu_s$ respectively, as shown in figure 3.5. Further, the OPLL is assumed to be an ideal OPLL with bandwidth f_L so that

$$G_{op}(f) = \begin{cases} \infty & \text{if} \quad f \le f_L, \\ 0 & \text{if} \quad f > f_L. \end{cases} \tag{3.5}$$

Using equation (3.1) and assuming that the effect of the master laser RIN is negligible (as is the case when $\phi_{e0} \ll 1$ even if the RIN is nonnegligible), we obtain

$$S_\nu^{lock}(f) = \begin{cases} \Delta\nu_m/2\pi & \text{if} \quad f \le f_L, \\ \Delta\nu_s/2\pi & \text{if} \quad f > f_L, \end{cases} \tag{3.6}$$

as shown by the dashed curve in figure 3.5. We denote the reduction in linewidth by β:

$$\beta = \Delta\nu_s - \Delta\nu_m. \tag{3.7}$$

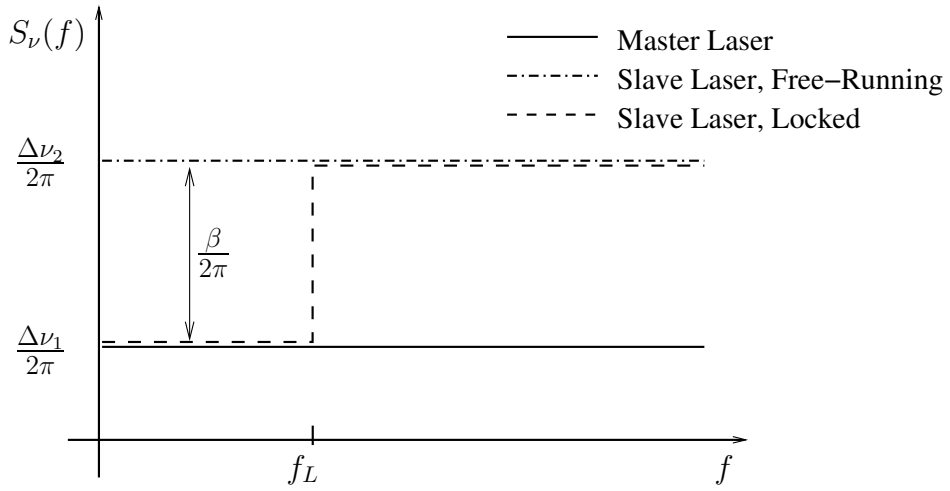

Figure 3.5. Model of the power spectral density of the frequency noise of the master laser and the free-running and locked slave laser. The OPLL is assumed to be "ideal" with a loop bandwidth f_L.

The accumulated phase noise $\Delta\phi\,(t, T_d)$ in equation (3.3) for a free-running laser is the result of a large number of independent spontaneous emission events that occur in the time interval $(t - T_d, t)$, and it follows from the central limit theorem that it is a zero-mean Gaussian random process. In order to simplify the mathematics, it is also assumed that $\Delta\phi\,(t, T_d)$ is a (wide-sense) stationary process. It is a property of Gaussian random variables [90] that the random process obtained by passing a Gaussian random process is passed through a linear time invariant (LTI) filter is also a Gaussian random process.[1] Therefore, the phase noise of a the phase-locked SCL also follows Gaussian statistics. Writing down the autocorrelation of $\Delta\phi\,(t, T_d)$ and taking the Fourier transform, we derive the relation between its spectral density and that of the frequency noise [72, 91]:

$$S_{\Delta\phi(t,T_d)}\,(f) = 4\pi^2\,T_d^2\,S_\nu(f)\,\mathrm{sinc}^2\,(\pi f T_d)\,, \tag{3.8}$$

[1]This follows from the property that a linear combination of Gaussian random process is a Gaussian random process [90, p. 38].

with $\mathrm{sinc}(x) \doteq \dfrac{\sin x}{x}$. The variance of the accumulated phase is therefore given by

$$\sigma^2_{\Delta\phi}(T_d) = 4\pi T_d \int_{-\infty}^{\infty} S_\nu(f)\,\mathrm{sinc}^2(\pi f T_d)\ \pi T_d\, df. \tag{3.9}$$

Since $\Delta\phi(t, T_d)$ is a zero-mean Gaussian process, its statistics (and therefore the statistics of the photocurrent in equation (3.3)) are completely determined by equation (3.9).

We now calculate $\sigma^2_{\Delta\phi}(T_d)$ for the case of a free-running laser and a phase-locked laser with frequency noise spectra given by equations (3.4) and (3.6) respectively. For a free-running laser, we have from equation (3.9),

$$\begin{aligned}\sigma^2_{\Delta\phi}(T_d) &= 2\Delta\nu T_d \int_{-\infty}^{\infty} \mathrm{sinc}^2(x)\ dx \\ &= 2\pi\Delta\nu T_d \\ &= \frac{2T_d}{t_c}.\end{aligned} \tag{3.10}$$

Here $t_c = 1/(\pi\Delta\nu)$ is the coherence time of the laser, defined as the time taken for the accumulated phase noise to achieve a root-mean-squared (rms) value of $\sqrt{2}$ radians. This definition of coherence time is a little arbitrary, and other definitions have been used by different authors in literature. The variance of the accumulated phase noise therefore increases linearly with observation time. (Note that $\sigma^2_{\Delta\phi}(T_d)$ is an even function of T_d.) It is interesting to note that experimental measurements of $\sigma^2_{\Delta\phi}(T_d)$ show the linear trend of equation (3.10) but have additional damped oscillations at low values of T_d corresponding to the relaxation resonance frequency [92].

For the phase-locked slave laser, we have

$$\begin{aligned}\sigma^2_{\Delta\phi}(T_d) &= 4\pi T_d \int_{-\infty}^{\infty} S_\nu^{lock}(f)\,\mathrm{sinc}^2(\pi f T_d)\ \pi T_d\, df \\ &= 2\Delta\nu_s T_d \int_{-\infty}^{\infty} \mathrm{sinc}^2(x)\ dx - 2\beta T_d \int_{-\pi f_L T_d}^{\pi f_L T_d} \mathrm{sinc}^2(x)\ dx \\ &= 2\pi\Delta\nu_2 T_d - 4\beta T_d\, g(\pi f_L T_d),\end{aligned} \tag{3.11}$$

where we define the function

$$g(x) \doteq \int_0^x \operatorname{sinc}^2(\alpha)\, d\alpha. \tag{3.12}$$

The second term in equation (3.11) quantifies the improvement in phase noise (or coherence) due to phase-locking. To calculate $g(x)$, we recast equation (3.12) in the form

$$\begin{aligned} g(x) &= \int_0^x \frac{\sin^2\alpha}{\alpha^2}\, d\alpha \\ &= -\frac{\sin^2\alpha}{\alpha}\bigg|_0^x + \int_0^x \frac{\sin 2\alpha}{\alpha}\, d\alpha \\ &= -\frac{\sin^2 x}{x} + \mathrm{Si}(2x), \end{aligned} \tag{3.13}$$

where $\mathrm{Si}(x)$ is the well-known sine integral [93] $\displaystyle\int_0^x \frac{\sin\alpha}{\alpha}\, d\alpha$, whose values have been numerically computed. The function $g(.)$ has the limits $g(0) = 0$ and $\lim\limits_{x\to\infty} g(x) = \pi/2$.

From equation (3.11), for low values of T_d ($\pi f_L T_d \ll 1$), $\operatorname{sinc}^2(x) \approx 1$, and we have $\sigma^2_{\Delta\phi}(T_d) \approx 2\pi\Delta\nu_s T_d$, whereas for $\pi f_L T_d \gg 1$ we have $g(\pi f_L T_d) \approx \pi/2$ and $\sigma^2_{\Delta\phi}(T_d) \approx 2\pi\Delta\nu_m T_d$. Therefore the variance of the accumulated phase noise follows that of the free-running slave laser for low values of T_d and that of the master laser for large values of T_d. The variation of $\sigma^2_{\Delta\phi}(T_d)$ vs. T_d is numerically calculated and plotted in figure 3.6. The values used in the calculation are $\Delta\nu_1 = 5$ kHz and $\Delta\nu_2 = 500$ kHz. The loop bandwidth f_L is varied between 1 and 100 MHz. It can be seen that $\sigma^2_{\Delta\phi}(T_d)$ follows the free-running slave laser for $T_d \lesssim \dfrac{1}{10 f_L}$ and is approximately equal to that of the master laser for $T_d \gtrsim \dfrac{100}{f_L}$.

3.3.2.2 Spectrum of the Laser Field

It is instructive to first calculate the shape of the electric field spectrum, i.e., the spectrum of $e(t) = \cos(\omega_0 t + \phi(t))$ for a free-running and phase-locked laser. To do

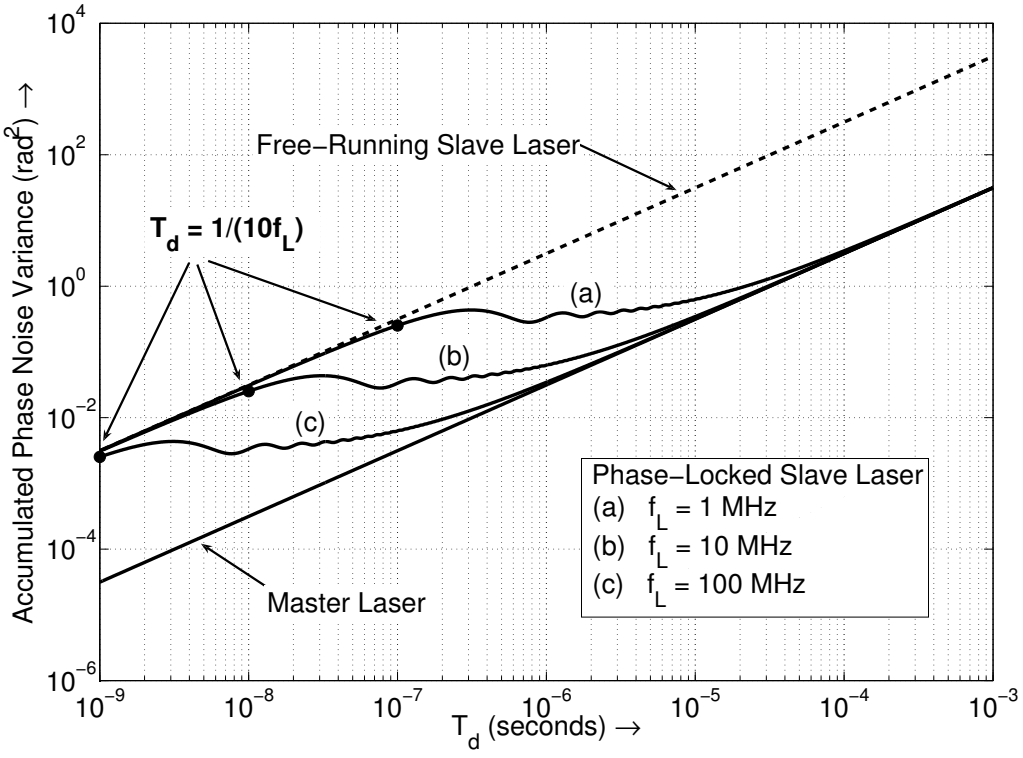

Figure 3.6. Variation of the accumulated phase error variance $\sigma^2_{\Delta\phi}(T_d)$ vs. interferometer delay time T_d for various values of the loop bandwidth f_L. The markers correspond to the delay time $T_d = 1/(10f_L)$. The linewidths of the master laser and the free-running slave laser are assumed to be 5 and 500 kHz respectively.

this, we write down the autocorrelation of the electric field:

$$\begin{aligned} R_e(\tau) &= \langle e(t)e(t-\tau)\rangle \\ &= \frac{1}{2}\left\langle \cos\left(2\omega_0 t + \omega_0\tau + \phi(t) + \phi(t-\tau)\right) + \cos(\omega_0\tau + \Delta\phi(t,\tau)\right\rangle \\ &= \frac{1}{2}\left\langle \cos(\omega_0\tau)\cos\left(\Delta\phi(t,\tau)\right)\right\rangle \\ &= \frac{\cos(\omega_0\tau)}{2}\exp\left(-\frac{\sigma^2_{\Delta\phi}(\tau)}{2}\right), \end{aligned} \tag{3.14}$$

where we have assumed that $\phi(t)$ is constant over one optical cycle and used the result $\langle \cos X\rangle = \exp\left(-\sigma_X^2/2\right)$ for a Gaussian random variable X.[2] From the Wiener-Khintchine theorem, the spectrum of the electric field is given by the Fourier transform of equation (3.14). The $\cos(\omega_0\tau)$ term simply shifts the spectrum of $e^{-\sigma^2_{\Delta\phi}(\tau)/2}$ to the center frequency ω_0. We define the spectrum at baseband by

$$S_{e,b}(f) = \mathcal{F}\left\{\exp\left(-\frac{\sigma^2_{\Delta\phi}(\tau)}{2}\right)\right\}, \tag{3.15}$$

so that the two-sided spectral density of the field $S_e(f)$ is given by

$$S_e(f) = \frac{1}{4}\left(S_{e,b}\left(f - \frac{\omega_0}{2\pi}\right) + S_{e,b}\left(f + \frac{\omega_0}{2\pi}\right)\right). \tag{3.16}$$

For a free-running laser, equations (3.10) and (3.15) yields the expected Lorenzian lineshape

$$S_{e,b}(f) = \frac{2}{\pi\Delta\nu}\frac{1}{1 + (2f/\Delta\nu)^2}. \tag{3.17}$$

For the phase-locked laser, the field lineshape is calculated using equations (3.11) and (3.15) and is shown in figure 3.7 for different values of the loop bandwidth f_L. It can be seen that the lineshape of the phase-locked laser follows that of the free-running slave laser for frequencies $f \geq f_L$ and that of the master laser for frequencies $f \lesssim f_L$. This result is in very good agreement with the experimentally measured lineshapes in figure 3.2. We intuitively understand this result by noting that for sufficiently large

[2]This is easily derived by expanding the cosine in terms of complex exponentials and evaluating the expectation by completing squares.

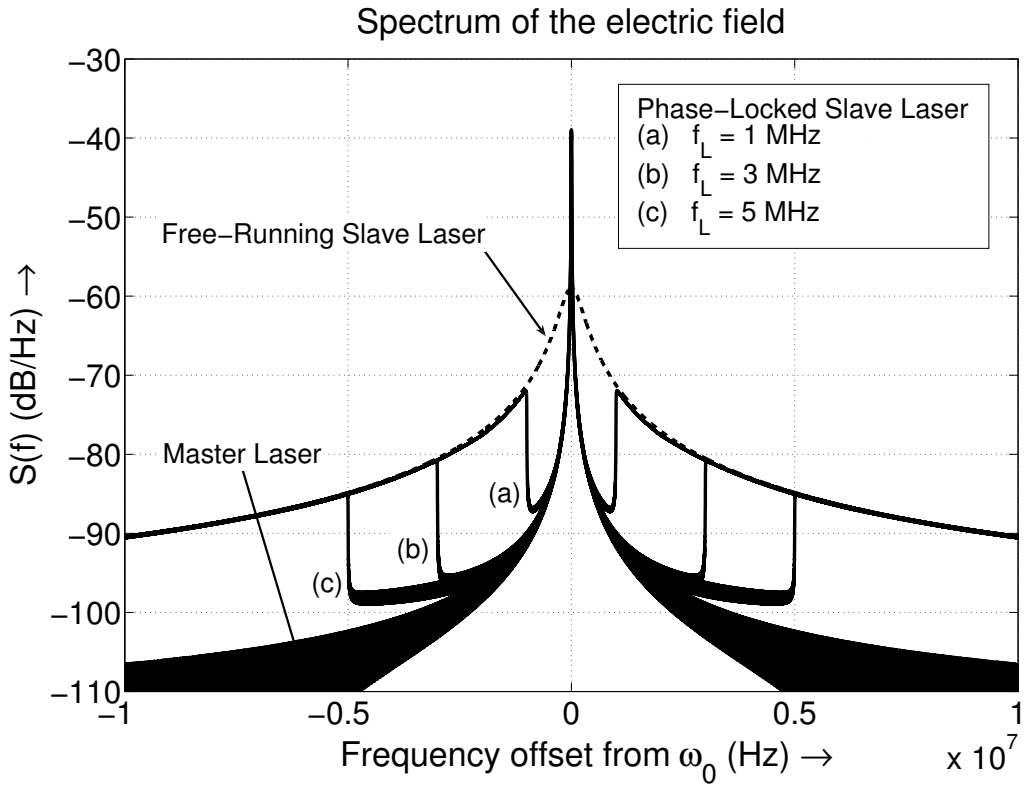

Figure 3.7. Spectral density of the optical field for different values of the loop bandwidth f_L, calculated using equation (3.15). The master laser and the free-running slave laser have Lorenzian lineshapes with FWHM 5 kHz and 500 kHz respectively.

frequencies, the phase noise is much smaller than one radian. We can therefore make the approximation $\cos(\omega_0 t + \phi(t)) \approx \cos(\omega_0 t) + \phi(t)\sin(\omega_0 t)$, and the behavior of the field spectrum in this frequency range is therefore the same as that of the spectrum of the phase noise.

3.3.2.3 Spectrum of the Detected Photocurrent

We now calculate the spectrum of the photocurrent detected in the experimental setup of figure 3.4, i.e., the spectrum of the current $i(t)$ in equation (3.3):

$$i(t) = \cos\left(\omega_0 T_d + \Omega t + \Delta\phi(t, T_d)\right).$$

We begin by deriving the autocorrelation of the photocurrent, similar to equation (3.14)

$$\begin{aligned} R_i(\tau) &= \langle i(t) i(t-\tau) \rangle \\ &= \langle \cos\left(\omega_0 T_d + \Omega t + \Delta\phi(t, T_d)\right) \cos\left(\omega_0 T_d + \Omega(t-\tau) + \Delta\phi(t-\tau, T_d)\right) \rangle \\ &= \frac{1}{2} \langle \cos\Omega\tau \, \cos\theta(t, T_d, \tau) \rangle \\ &= \frac{\cos\Omega\tau}{2} \exp\left(-\frac{\sigma_\theta^2(T_d, \tau)}{2}\right), \end{aligned} \tag{3.18}$$

where we define

$$\theta(t, T_d, \tau) \doteq \Delta\phi(t, T_d) - \Delta\phi(t-\tau, T_d). \tag{3.19}$$

In deriving equation (3.18), we have made the assumption that Ω is much larger than the laser linewidth, and used the fact that θ follows Gaussian statistics. The variance of θ is given by

$$\begin{aligned} \sigma_\theta^2(T_d, \tau) &= \left\langle \theta^2(t, T_d, \tau) \right\rangle \\ &= \left\langle \Delta\phi^2(t, T_d) + \Delta\phi^2(t-\tau, T_d) - 2\Delta\phi(t, T_d)\Delta\phi(t-\tau, T_d) \right\rangle \\ &= 2\sigma_{\Delta\phi}^2(T_d) - 2\left\langle \Delta\phi(t, T_d)\Delta\phi(t-\tau, T_d) \right\rangle. \end{aligned} \tag{3.20}$$

$$\begin{aligned}\langle \Delta\phi(t,T_d)\Delta\phi(t-\tau,T_d)\rangle &= \langle (\phi(t)-\phi(t-T_d))\,(\phi(t-\tau)-\phi(t-\tau-T_d))\rangle \\ &= \frac{1}{2}\left\langle \Delta\phi^2(t,\tau+T_d)+\Delta\phi^2(t-T_d,\tau-T_d)\right. \\ &\qquad \left. -\,\Delta\phi^2(t,\tau)-\Delta\phi^2(t-T_d,\tau)\right\rangle \\ &= \frac{1}{2}\sigma^2_{\Delta\phi}(\tau+T_d)+\frac{1}{2}\sigma^2_{\Delta\phi}(\tau-T_d)-\sigma^2_{\Delta\phi}(\tau)\,. \end{aligned} \tag{3.21}$$

Substituting back into equation (3.20), we have

$$\sigma^2_\theta(T_d,\tau) = 2\sigma^2_{\Delta\phi}(T_d)+2\sigma^2_{\Delta\phi}(\tau)-\sigma^2_{\Delta\phi}(\tau+T_d)-\sigma^2_{\Delta\phi}(\tau-T_d)\,. \tag{3.22}$$

We again define the baseband current spectrum,

$$S_{i,b}(f) = \mathcal{F}\left\{\exp\left(-\frac{\sigma^2_\theta(T_d,\tau)}{2}\right)\right\}, \tag{3.23}$$

so that the double sided spectral density of the photocurrent is given by

$$S_i(f) = \frac{1}{4}\left(S_{i,b}\left(f-\frac{\Omega}{2\pi}\right)+S_{i,b}\left(f+\frac{\Omega}{2\pi}\right)\right). \tag{3.24}$$

The case of a free-running laser has been studied previously by Richter et al. [83], and will be briefly rederived here. In this case, using $\sigma^2_{\Delta\phi}(\tau) = 2\pi\Delta\nu|\tau|$ from equation (3.10) in equation (3.22), we obtain

$$\begin{aligned}\sigma^2_\theta(T_d,\tau) &= 2\pi\Delta\nu\,(2|\tau|+2T_d-|\tau+T_d|-|\tau-T_d|) \\ &= \begin{cases} 4\pi\Delta\nu|\tau|, & |\tau|\le T_d, \\ 4\pi\Delta\nu T_d, & |\tau|>T_d, \end{cases}\end{aligned} \tag{3.25}$$

which leads to a spectral density

$$\begin{aligned}S_{i,b}(f) = e^{-2\pi\Delta\nu T_d}\,\delta(f) &+ \frac{1}{\pi\Delta\nu}\,\frac{1}{1+(f/\Delta\nu)^2} \\ &\times\left[1-e^{-2\pi\Delta\nu T_d}\left(\cos 2\pi f T_d+\pi\Delta\nu\,\frac{\sin 2\pi f T_d}{\pi f}\right)\right].\end{aligned} \tag{3.26}$$

The resultant spectra for various values of the delay time T_d are shown in figure 3.8, traces (i), (iii). For low values of T_d where $\Delta\nu T_d \ll 1/\pi$, the spectrum is characterized by a sharp delta function accompanied by a pedestal with oscillations. The period of these oscillations corresponds to the delay T_d, or in other words, to the free spectral range of the interferometer. As the value of $\Delta\nu T_d$ increases, the strength of the delta function relative to the pedestal reduces, until we finally obtain a Lorenzian profile for $\Delta\nu T_d \gg 1/\pi$. The FWHM of this Lorenzian is equal to $2\Delta\nu$, as can be expected from beating two identical distinct lasers with linewidths $\Delta\nu$.

For the phase-locked slave laser, we numerically calculate the spectra of the photocurrent using equations (3.23), (3.22) and (3.11). The results of the calculation are shown in figure 3.8. In general, the shape of the spectrum of the photocurrent using the phase-locked slave laser follows that of the master laser with the following important difference. For frequencies larger than the loop bandwidth f_L, the power spectral density of the phase-locked laser increases to the level of the free-running case. However, the features corresponding to the free spectral range of the interferometer are still present. *The improvement in the coherence of the phase-locked SCL manifests itself in the presence of the delta function even at large delay times where the free-running laser results in a Lorenzian output.*

In most practical sensing applications involving lasers, the delay time T_d is much smaller than the coherence time of the laser, in the regime shown in figure 3.8(a). In this case, the presence of a pedestal constitutes a deviation from the "ideal" case of a delta function, and represents unwanted noise in the interferometric sensing measurement. Comparing the spectra of the master laser and the phase-locked laser in figure 3.8(a), we see that the noise level is almost identical for small frequencies, but the phase-locked laser has greater noise for frequencies greater than the OPLL bandwidth. However, this additional noise level is still many orders of magnitude below the delta function, and is outside the signal bandwidth so that it can be filtered out using a narrow bandwidth electrical filter. The coherence-cloned slave SCL can therefore perform well as a substitute for the high-quality master laser.

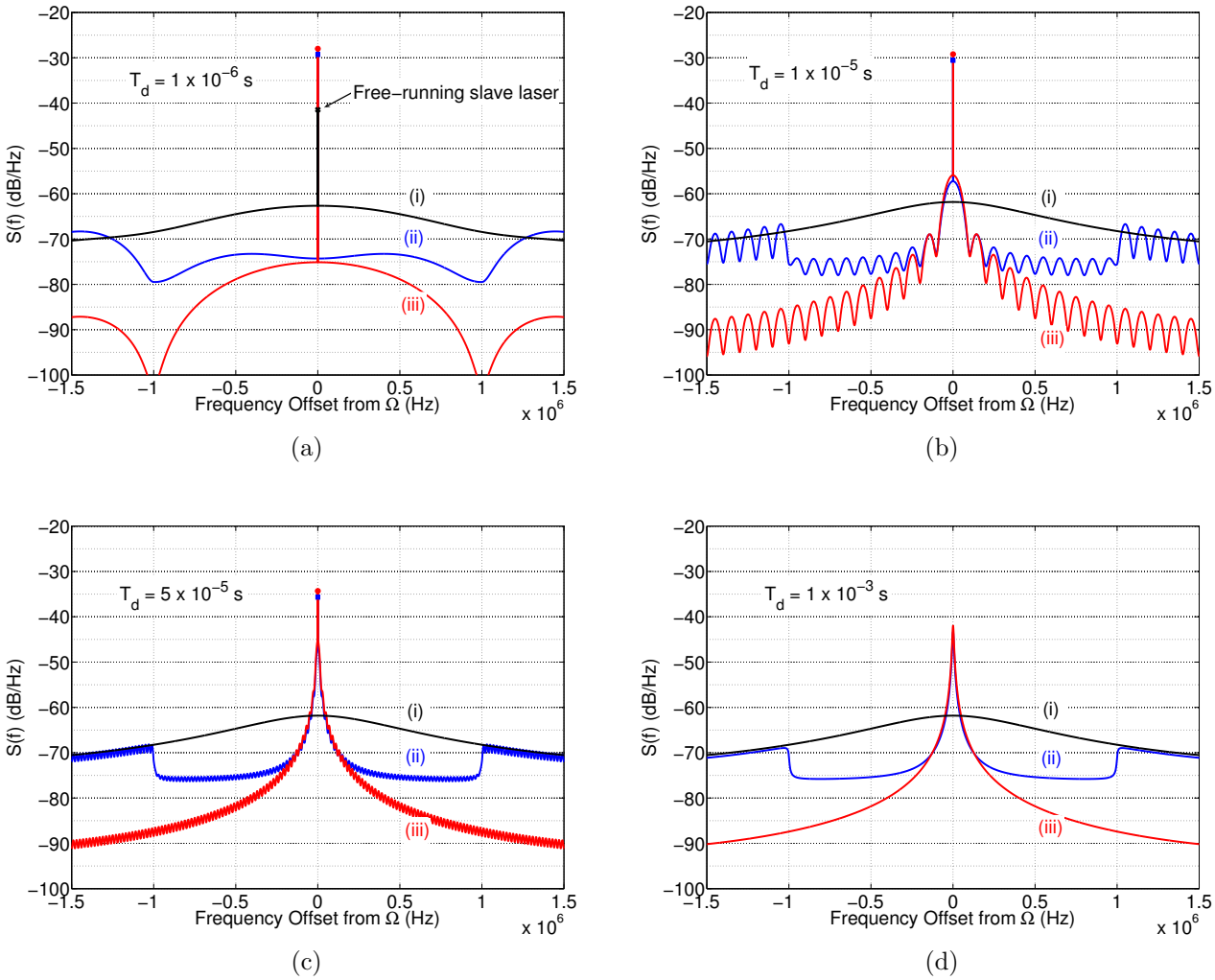

Figure 3.8. Spectral density of the detected photocurrent in a delayed self heterodyne experiment using the free-running slave laser (i), the phase-locked slave laser (ii), and the master laser (iii). The markers denote the height of the delta function. The spectra are calculated using equation (3.23), for different values of the interferometer delay T_d: (a) $T_d = 10^{-6}$ s. (b) $T_d = 10^{-5}$ s. (c)$T_d = 5$ x 10^{-5} s. (d)$T_d = 10^{-3}$ s. The master laser and free-running slave laser linewidths are assumed to be 5 and 500 kHz respectively, and the loop bandwidth is assumed to be $f_L = 1$ MHz.

3.3.3 Summary

In summary, we have demonstrated the concept of "coherence cloning," i.e. the cloning of the spectral properties of a high quality master laser to an inexpensive SCL using an OPLL, and shown that the cloned SCL can act as a substitute for the master laser in interferometric sensing applications. The bandwidth over which the spectrum is cloned is limited by physical factors such as the FM response of the SCL and the OPLL propagation delay. Using a simple model for the coherence cloning, we have investigated the effect of this limited bandwidth on the spectrum of the laser electrical field and on the result of interferometric experiments using the laser, which are common in many sensing applications. We have demonstrated that the spectrum of the field of the locked laser follows the master laser for frequencies lower than the loop bandwidth, and follows the free-running spectrum for higher frequencies. We have further shown that a similar behavior is observed in interferometric experiments. Since the additional noise due to the limited loop bandwidth appears at high frequencies greater than the loop bandwidth, it can be electronically filtered off using a narrow bandwidth filter.

While we have analyzed the effects of a coherence cloning approach using OPLLs, the results are valid for any general feedback-based linewidth narrowing approach, since the bandwidth of linewidth reduction is always finite and limited by the propagation delay in the feedback scheme.

3.4 Time-Domain Characterization of an OPLL

In the previous section, we have described the rigorous characterization of the performance of the OPLL by a measurement of the spectral density of the frequency noise of the lasers. In this section, we investigate the characterization of a heterodyne OPLL in the time domain using a frequency counter. This measurement technique, used widely in the characterization of oscillators [94], is simpler than the frequency-domain measurement of the phase noise, since it eliminates the need for stabilized

frequency discriminators. We also show that the measurement can be used to obtain a more accurate measurement of the residual phase error of the OPLL, σ_ϕ.

We will continue to assume that the master and the free-running slave laser have flat frequency noise spectra corresponding to Lorenzian lineshapes with FWHMs $\Delta\nu_m$ and $\Delta\nu_s$ respectively, as shown in figure 3.5, and that the OPLL is ideal with bandwidth f_L as given by equation (3.5):

$$G_{op}(f) = \begin{cases} \infty & \text{if} \quad f \leq f_L, \\ 0 & \text{if} \quad f > f_L. \end{cases}$$

Under these assumptions, equation (2.18) yields

$$\sigma_\phi^2 = \frac{\Delta\nu_m + \Delta\nu_s}{\pi f_L}. \tag{3.27}$$

Whereas a measurement of the spectral density is a thorough characterization of the phase (or frequency) noise of a signal, a simpler measurement, the Allan variance [94], is often used to characterize the stability and phase noise of oscillators. For an oscillator of frequency ν_0 and frequency noise $\nu(t)$, we define the fractional frequency fluctuation $y(t) = \nu(t)/\nu_0$. The Allan variance $\sigma_y^2(\tau)$ is defined as the two-sample variance of the fractional frequency fluctuations [95], i.e.,

$$\sigma_y^2(\tau) = \frac{1}{2}\left\langle (\bar{y}_2 - \bar{y}_1)^2 \right\rangle, \tag{3.28}$$

where $\bar{y}_1$ and $\bar{y}_2$ are consecutive measurements of the average value of $y(t)$, averaged over a gate period τ. As before, $\langle . \rangle$ is the expectation value. There is no "dead time" between the measurements $\bar{y}_1$ and $\bar{y}_2$. In practice, a frequency counter is used to measure the average fractional frequency fluctuation $\bar{y}$.

The Allan variance can be related to the spectral density of the phase noise fol-

lowing a straightforward derivation [95]. From equation (3.28),

$$\begin{aligned}\sigma_y^2(\tau) &= \frac{1}{2}\left\langle\left(\frac{1}{\tau}\int_t^{t+\tau} y(t')\,dt' - \frac{1}{\tau}\int_{t-\tau}^{t} y(t')\,dt'\right)^2\right\rangle \\ &= \left\langle\left(\int_{-\infty}^{\infty} y(t')h_\tau(t-t')\,dt'\right)^2\right\rangle, \end{aligned} \tag{3.29}$$

with

$$h_\tau(t) = \begin{cases} -\dfrac{1}{\sqrt{2}\tau} & \text{for} \quad -\tau < t < 0, \\ +\dfrac{1}{\sqrt{2}\tau} & \text{for} \quad 0 \le t < \tau, \\ 0 & \text{otherwise.} \end{cases} \tag{3.30}$$

In the frequency domain, equation (3.29) can be written as

$$\begin{aligned}\sigma_y^2(\tau) &= \int_{-\infty}^{\infty} |H_\tau(f)|^2\, S_y(f)\,df \\ &= 4\int_0^{\infty} \frac{\sin^4(\pi\tau f)}{(\pi\tau f)^2} S_y(f)\,df, \end{aligned} \tag{3.31}$$

where we have calculated the Fourier transform $H_\tau(f)$ of $h_\tau(t)$. By definition, the spectral density of the fractional frequency fluctuations is

$$S_y(f) = \frac{1}{\nu_0^2} S_\nu(f) = \left(\frac{f}{\nu_0}\right)^2 S_\phi(f). \tag{3.32}$$

The Allan variance can therefore also be written as

$$\sigma_y^2(\tau) = \left(\frac{2}{\pi\tau\nu_0}\right)^2 \int_0^{\infty} \sin^4(\pi\tau f) S_\phi(f)\,df, \tag{3.33}$$

3.4.1 Experiment

The statistics of the relative frequency noise between the slave laser and the master laser were measured in this experiment. The Allan variance of the slave laser is the sum of the Allan variance of the master laser and the measured relative variance. Since the principal idea behind phase-locking is to clone the properties of the slave laser to

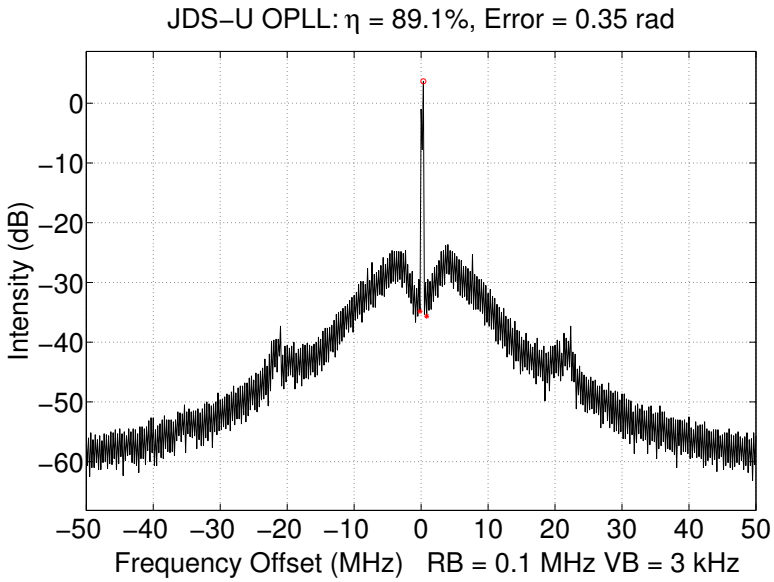

Figure 3.9. Spectrum of the beat signal between the phase-locked slave SCL and the master laser.

the master laser, the measurement of the relative stability sufficiently characterizes the OPLL. A commercial DFB laser (JDS-Uniphase) was phase-locked to a high quality fiber laser (NP Photonics) in a heterodyne OPLL, with an offset frequency $\nu_0 = 800$ MHz. An RF spectrum analyzer and a frequency counter (SR620, Stanford Research Systems, Sunnyvale, CA) were used to characterize the beat signal between the slave and master lasers.

The measured beat spectrum between the phase-locked SCL and the master laser is shown in figure 3.9, and by integrating the noise power over a bandwidth of ± 50 MHz around the offset frequency, we obtain $\eta = 89.1\%$ and $\sigma_\phi = 0.35$ rad. Note that the residual phase error calculated from this measurement is typically a function of the bandwidth over which the noise is integrated, and a large bandwidth has to be chosen in order to achieve accurate results.

3.4.1.1 Allan Variance and Stability

A frequency counter was used to measure the Allan variance of the beat signal between the master laser and the slave laser, for gate times between $\tau = 20$ ns and $\tau = 0.5$ s. The expectation value in equation (3.28) was calculated by averaging over 1000

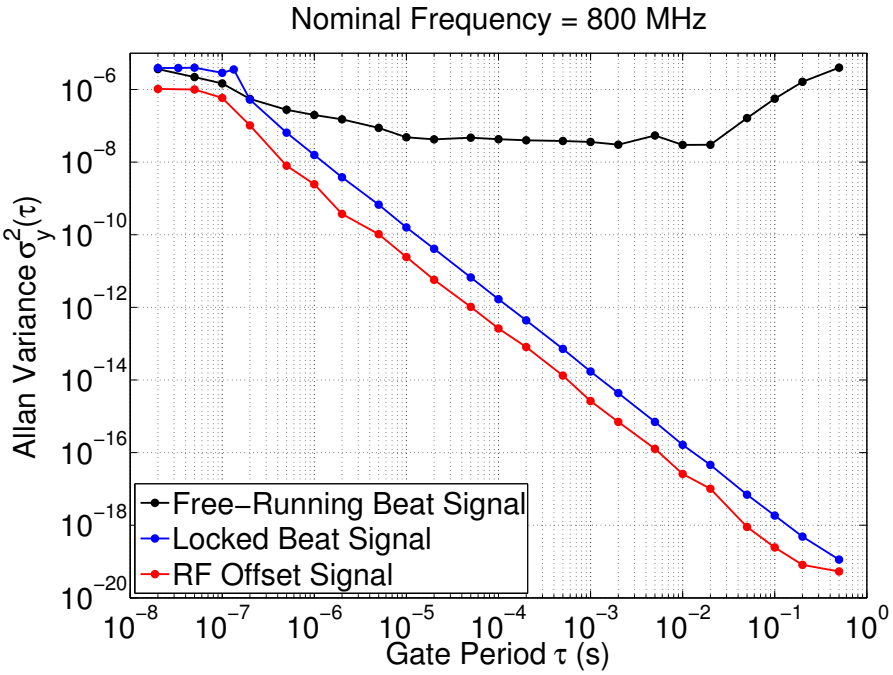

Figure 3.10. Measured Allan variance of the beat signal between the slave and master lasers for the locked and unlocked cases. The variance of the RF offset signal is also shown.

measurements. The results are plotted in figure 3.10. The free-running beat signal displays a large variance, which increases for large gate periods. Such a behavior indicates that the frequency noise spectrum of the slave laser is not flat; rather, the laser displays flicker frequency noise ($S_\nu(f) \sim f^{-1}$) or a random-walk type of frequency noise ($S_\nu(f) \sim f^{-2}$) [95]. This observation is consistent with the measured frequency spectrum of the free-running slave laser (figure 3.3), which shows that the frequency noise spectrum is not flat at low frequencies. The measured Allan variance of the phase-locked laser shows a marked improvement over the free-running case for measurement time scales larger than the inverse of the loop bandwidth (approximately 1–5 MHz), demonstrating the ability of the OPLL to improve the long-term stability of the slave semiconductor laser. The Allan variance of the offset signal is typically an order of magnitude smaller than the variance of the phase-locked beat signal, validating the assumption that the phase noise of the offset signal may be neglected in the analysis.

To understand the behavior of the laser beat signal for the phase-locked case,

we consider the simplified model of the OPLL introduced in equation (3.5). Using equations (2.16) and (3.5) in equation (3.33), we obtain

$$\begin{aligned}\sigma_y^2(\tau) &= \left(\frac{2}{\pi\tau\nu_0}\right)^2 \int_0^\infty \sin^4(\pi\tau f) S_\phi^e(f)\, df \\ &= \left(\frac{2}{\pi\tau\nu_0}\right)^2 \int_{f_L}^\infty \sin^4(\pi\tau f) \frac{\Delta\nu_m + \Delta\nu_s}{2\pi f^2}\, df\end{aligned}$$

$$\sigma_y^2(\tau) = \frac{2(\Delta\nu_m + \Delta\nu_s)}{\pi^2\tau\nu_0^2} \int_{\pi\tau f_L}^\infty \frac{\sin^4 x}{x^2}\, dx. \tag{3.34}$$

To evaluate the integral above, we note that

$$\sin^4 x = \frac{3}{8} + \frac{1}{8}\cos 4x - \frac{1}{2}\cos 2x, \tag{3.35}$$

and

$$\begin{aligned}\int_a^\infty \frac{\cos x}{x^2}\, dx &= -\frac{\cos x}{x}\Big|_a^\infty - \int_a^\infty \frac{\sin x}{x}\, dx \\ &= \frac{\cos a}{a} - \left(\frac{\pi}{2} - \int_0^a \frac{\sin x}{x}\, dx\right) \\ &= \frac{\cos a}{a} + \mathrm{Si}(a) - \frac{\pi}{2},\end{aligned} \tag{3.36}$$

where $\mathrm{Si}(x)$ is the sine integral [93]. The integral in equation (3.34) is then given by (with $a = \pi\tau f_L$)

$$\begin{aligned}\int_a^\infty \frac{\sin^4 x}{x^2}\, dx &= \int_a^\infty \left(\frac{3}{8x^2} + \frac{\cos 4x}{8x^2} - \frac{\cos 2x}{2x^2}\right) dx \\ &= \frac{1}{a}\left(\frac{3}{8} + \frac{1}{8}\cos 4a - \frac{1}{2}\cos 2a\right) + \frac{\pi}{4} + \frac{1}{2}\mathrm{Si}(4a) - \mathrm{Si}(2a) \\ &= \frac{\sin^4 a}{a} + \frac{\pi}{4} + \frac{1}{2}\mathrm{Si}(4a) - \mathrm{Si}(2a).\end{aligned} \tag{3.37}$$

The Allan variance is therefore given by

$$\sigma_y^2(\tau) = \frac{2(\Delta\nu_m + \Delta\nu_s)}{\pi^2\tau\nu_0^2}\left(\frac{\sin^4 \pi\tau f_L}{\pi\tau f_L} + \frac{\pi}{4} + \frac{1}{2}\mathrm{Si}(4\pi\tau f_L) - \mathrm{Si}(2\pi\tau f_L)\right). \tag{3.38}$$

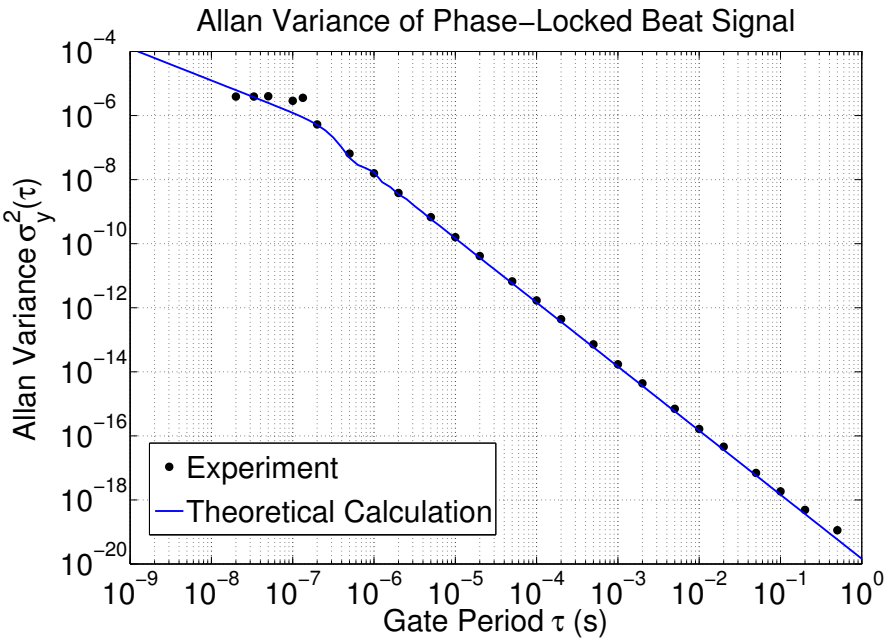

Figure 3.11. Measured Allan variance of the beat signal between the phase-locked slave laser and the master laser, and the theoretical calculation based on equation (3.38). Experimental values of $\sigma_\phi = 0.35$ rad and $\Delta\nu_m + \Delta\nu_s = 0.5$ MHz were used in the calculation.

The measured Allan variance and the theoretical calculation using equation (3.38) are plotted in figure 3.11. The loop bandwidth is calculated from the measured residual phase error $\sigma_\phi = 0.35$ rad and the measured linewidth $\Delta\nu_m + \Delta\nu_s = 0.5$ MHz using equation (3.27). The calculated loop bandwidth is $f_L = 1.3$ MHz. *Note that no freely varying parameters were used to fit the calculation to the data.* The theoretical calculations match the experimental data well, especially at larger gate periods. The discrepancy at lower gate periods (smaller than the inverse of the loop bandwidth) is probably due to a combination of factors: (i) the inaccuracy of the simplified OPLL model (3.5) and (ii) the limitation of the frequency counter in measuring frequencies at very short gate periods. Further investigation is necessary to explain this discrepancy, but the excellent fit at longer gate times suggests that the measurement of the Allan variance is can be an accurate tool to characterize the performance of an OPLL.

3.4.1.2 Residual Phase Error, Revisited

In the previous section, we have considered a particular, simplified, model for the OPLL and calculated the Allan variance of the laser beat signal based on this model. In this section, we will show that the Allan variance measurement can be used to calculate the residual phase error in the OPLL, *irrespective of the shape of the loop transfer function* $G_{op}(f)$. We will only assume that the loop suppresses all the phase noise at frequencies much smaller than the loop bandwidth; this assumption is clearly valid as seen in figure 3.3. The residual phase error in the loop is a key metric in many applications, and its accurate measurement is essential.

We start with equation (3.33):

$$\begin{aligned} \sigma_y^2(\tau) &= \left(\frac{2}{\pi\tau\nu_0}\right)^2 \int_0^\infty \sin^4(\pi\tau f) S_\phi^e(f)\, df \\ &\simeq \left(\frac{2}{\pi\tau\nu_0}\right)^2 \int_{f_1}^\infty \sin^4(\pi\tau f) S_\phi^e(f)\, df \end{aligned} \tag{3.39}$$

for some f_1 much smaller than the loop bandwidth. Let us now choose $\tau \gg 1/f_1$. Then, for frequencies over which the integration is carried out, we have $2\pi\tau f \gg 2\pi$, so that the $\sin^4(.)$ function is rapidly oscillating. The spectral density $S_\phi^e(f)$ does not change appreciably over one period of oscillation, and we can approximate the Allan variance as

$$\begin{aligned} \sigma_y^2(\tau) &\simeq \left(\frac{2}{\pi\tau\nu_0}\right)^2 \left(\frac{1}{\pi}\int_0^\pi \sin^4 x\, dx\right) \int_{f_1}^\infty S_\phi^e(f)\, df \\ &= \left(\frac{3}{2\pi^2\tau^2\nu_0^2}\right) \int_{f_1}^\infty S_\phi^e(f)\, df. \end{aligned} \tag{3.40}$$

From equation (2.15), the integral above is simply half the variance of the residual phase error in the loop, since the spectrum of the phase error is zero at low frequencies. We therefore have a relation between the loop residual phase error and the Allan variance of the laser beat note:

$$\sigma_\phi^2 = \frac{4\pi^2\tau^2\nu_0^2}{3}\sigma_y^2(\tau), \quad \text{for } (1/\tau) \ll \text{ the loop bandwidth.} \tag{3.41}$$

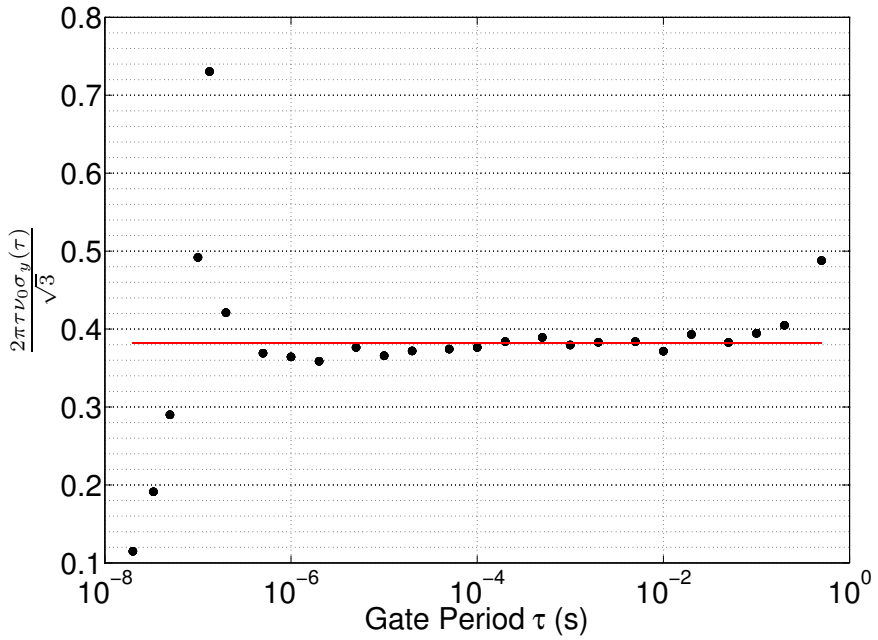

Figure 3.12. Residual phase error calculated from the measured Allan variance using equation (3.41). Using $\tau \gg 10^{-6}$, we obtain $\sigma_\phi = 0.38$ rad.

From the experimental measurement of $\sigma_y(\tau)$, the value $2\pi\tau\nu_0\sigma_y(\tau)/\sqrt{3}$ is calculated and plotted in figure 3.12. It is clear that for large-enough τ, this measurement yields a constant value for the standard deviation of the residual OPLL phase error, here equal to 0.38 rad. This value is about 10% higher than the value calculated from the spectrum in figure 3.9, demonstrating that the spectral method of phase-error calculation tends to underestimate the actual value.

3.4.2 Summary

In this section, we have investigated the use of a frequency counter for the time-domain characterization of the performance of an OPLL. The measured Allan variance of the beat signal between the master laser and the slave SCL clearly shows the improvement in stability and the reduction of the frequency noise of the slave laser by the process of phase-locking. We have shown that theoretical calculations of the Allan variance using a simplified model of an ideal OPLL are in very good agreement with the experimentally measured values. Finally, we have shown that the Allan variance

measurement at gate periods much longer than the inverse loop bandwidth of the OPLL can be used to calculate the residual phase error in the loop, which is an important metric in determining loop stability. The residual phase error measured using this method is larger than the value estimated from spectral measurements of the laser by about 10%, a discrepancy attributed to the finite bandwidth of the spectral measurement.